368 *Macromolecules* **2011**, *44*, 368–374
DOI: 10.1021/ma102032t

Macromolecules
ARTICLE

Entropic Effects on the Mechanical Behavior of Dry Polymer Brushes During Nanoindentation by Atomic Force Microscopy

Davide Tranchida,*,† Elena Sperotto,† Antoine Chateauminois,‡ and Holger Schönherr*,†

†*Department of Physical Chemistry I, University of Siegen, Adolf-Reichwein-Strasse 2, 57076 Siegen, Germany, and* ‡*Laboratoire de Physico-Chimie des Polymères et des Milieux Disperses, UMR CNRS 7615 Ecole Supérieure de Physique et Chimie Industrielles (ESPCI), 10 rue Vauquelin, 75231 Paris Cedex 05, France*

Received September 1, 2010; Revised Manuscript Received December 7, 2010

ABSTRACT: We report on the dependence of the mechanical properties of confined polymers on the film architecture. Compared to spin-coated films, grafted polymer brushes showed higher elastic moduli, which is attributed to entropy effects, and required higher loads to achieve the same residual indentation depth when compared to spin-coated samples. The contribution of entropy changes to the mechanical response of brushes was evaluated. Although qualitative, this study tries for the first time to evaluate this entropic contribution. Therefore, the role of morphology and architecture of the polymer films during mechanical deformation is highlighted, showing that the change of surface thermodynamic properties (entropy in particular) changes accordingly the nanometer scale mechanical properties.

1. Introduction

Surface-grafted polymers[1,2] allow one to design specific functional systems for various applications due to the synthetic flexibility, chemical robustness, and the high grafting densities obtained. They also offer the possibility to tune the morphology and final properties of modified surfaces, such as friction, wettability, or biocompatibility,[3−5] among others. In particular, applications to colloidal stabilization,[6,7] adhesion,[8] or lubrication[9] require a profound knowledge of surface mechanical performance.

Although nanoscale mechanical properties of polymers have been studied in detail, the peculiar morphologies obtained when considering polymer brushes pose some challenges and much less is known about their nanoscale mechanical properties.[10] The mobility of polymer chains at the interface[11] and nanoconfinement effects,[12] inherent, e.g., to ultrathin films, as well as entropic penalty contributions,[13] may give rise to unexpected and, compared to the bulk, altered behavior.

One typical example for this altered behavior is the glass transition temperature (T_g) of ultrathin free-standing or substrate-supported films.[14−16] The effect of the two interfaces, i.e. the interface of the polymer with the substrate and the interface with the air, on chain and segment mobility was shown to provide a plausible explanation for the observed depressed or elevated values of T_g.[17] Frank and co-workers addressed the relation of polymer thin film architecture and T_g in substrate supported films and concluded that the architecture had negligible influence on the T_g measured.[18] In addition, the coil configuration of the individual polymers was concluded to remain unaffected.

Apart from T_g, the confinement of polymers in ultrathin films may also significantly affect the films' mechanical properties. Previously, the surface forces apparatus (SFA)[19] and the atomic force microscope (AFM)[20] were applied to test the mechanical properties of polymer brushes swollen in good solvents. In these experiments fundamental information on the adhesion behavior and the chain conformation of polymer brushes was gained and compared to moderately dense brushes prepared by adsorption techniques. Mechanical stretching of single chains picked up by the AFM tip was also reported.[20]

Although these reports provide interesting hints on solvent-swollen systems, an exhaustive nanoscale mechanical characterization of dry polymer brushes in the glassy state, e.g., by AFM and contact mechanics, taking into account both elastic and plastic properties is still missing. In particular the interesting question of the dependence of the mechanical properties on the film architecture has remained unanswered to date.

Previously, dried poly(methyl methacrylate) (PMMA) brushes were studied on a larger scale by electromechanical interferometry, i.e., by measuring the plate compressibility of the films.[21] Urayama et al.[21] compared the mechanical behavior of spin-coated and grafted brush samples at temperatures around and above the glass-to-rubber transition temperature. These authors explained the higher resistance to compression and the considerable effect of entanglements by means of rubber elasticity theory and the Edwards−Vilgis slip-link model.[22] However, due to experimental limitations related to the low compressibility of glassy films and their limited thicknesses the anticipated differences in mechanical behavior among spin-coated and grafted PMMA films remained elusive.

In addition, surface wrinkling was used to show that the Young's modulus of poly(2-hydroxyethyl methacrylate) brush layers grafted on poly(dimethylsiloxane), PDMS are insensitive to film thickness.[23]

As a further approach to address mechanical properties of thin polymer films quantitatively, AFM nanoindentation represents often a most adequate tool for studying 3-D compressive properties, i.e., not only along the vertical direction of grafted chains.[24] Because of the ability to measure very small applied loads[25] and resulting penetration depths, AFM nanoindentation allowed in the past to link the morphology of polymers to their viscoelastic[26] and elastic[27] mechanical properties, as well as to characterize nanophases.[28] AFM based nanoindentation can be regarded as a complementary approach, since the mapping of mechanical properties of inhomogeneous samples is feasible, as well as the testing of brush films deposited on hard surfaces.

*Corresponding authors. E-mail: (H.S.) schoenherr@chemie.uni-siegen.de; (D.T.) tranchida@chemie.uni-siegen.de.

 Published on Web 12/23/2010

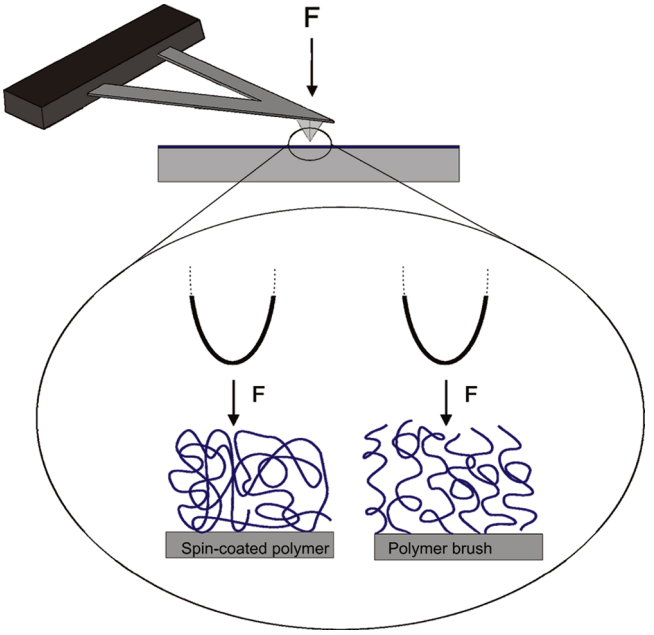

Figure 1. Schematic of AFM-based nanoindentation of ultrathin PMMA films obtained by spin-coating and SIP, respectively.

Interestingly, polymer brushes were only seldom studied in the past by AFM nanoindentation and contradictory results were reported. For example, the Young's moduli of tethered poly(styrene-*co*-2,3,4,5,6-pentafluorostyrene) (PSF) and poly(methyl acrylate) (PMA) chains were reported to be identical to the corresponding spin-coated samples.[29] By contrast, poly(styrene) brushes showed higher elastic moduli than the corresponding spin-coated samples and also better resistance to scratching in large scale scratch tests, which address a measurement of the films' plastic properties.[30]

In this article, we report on AFM nanoindentation measurements performed on grafted and spin-coated glassy PMMA films (Figure 1) to unravel qualitatively and quantitatively the effect of the polymer film architecture on the elastic and plastic properties of the films. In particular the differences among annealed spin-coated PMMA films and PMMA brushes obtained by surface-initiated polymerization (SIP) were compared. Noticeable differences in the elastic and plastic behavior on the nanometer scale[30] are explained based on a discussion of the thermodynamics of deformation.

2. Results

In this part, we will show differences in the mechanical behavior, i.e., measured Young's modulus and load required to induce the same residual depth, in order to justify the further study on the role of entropy changes to the deformation. Dealing with thin films, the effect of the substrate is unavoidable and precautions on the choice of film thicknesses, which will be discussed in the following, have been taken. The problem of identifying and minimizing substrate effects is indeed of great recent interest and a number of approaches have been proposed, both by theory, numerical simulations, and phenomenological approaches.[31−45]

The elastic and plastic properties of spin-coated and subsequently annealed PMMA films and corresponding brushes obtained by SIP were measured in AFM force-displacement curves. We compared the data of six different PMMA samples with different structure studied with different methods: (i) Macroscopic DMTA analysis (data from ref 46), AFM nanoindentations on (ii) a bulk sample (data from ref 46), (iii) a thin film on silicon obtained by spin-coating (150 nm thickness), (iv) a thin film on silicon obtained by spin-coating (70 nm thickness), and finally (v, vi) two grafted PMMA brushes on gold (similar thickness of 150 and 200 nm).

Following ref 46, a phenomenological elastic index ξ, bounded between zero and one in the ideal cases of rigid plastic behavior and elastic behavior, respectively, can be calculated as one minus the ratio of the residual indentation depth left behind the indenter and the maximum penetration depth.

In our present work, an index ξ as high as 0.80 was found for the spin-coated samples and the bulk sample. Therefore, the residual depth was 5 times smaller than the penetration under full load, giving the reader the feeling of the elastic contributions to the nanoindentation probably also related to the increase of yield stress at the high deformation rate achieved during the nanoindentation. In the case of the grafted film, the index ξ was estimated to be ~0.85. It is worth to mention that these values for ξ match the ones found for the bulk sample[46] therefore pointing at negligible substrate effects since, intuitively, when the stress field reaches the hard substrate, it causes purely elastic deformations that are completely recovered upon unloading thus increasing the ξ value with respect to nanoindentation of a bulky sample.

To quantify the force data and to model the contact mechanics, we used Sneddon's model with a parabolic indenter shape.[46,47] The tip shape was experimentally determined using blind reconstruction. This choice is motivated by previous results that highlighted the possibility to evaluate the elastic modulus of polymeric samples from AFM nanoindentations for a wide range of polymer states and morphologies, from glassy to semicrystalline to mesomorphic ones.[46] Sneddon's theory models the sample as an isotropic elastic half-space.

The evaluation of the Young's modulus of the films with Sneddon's model is in general accurate in the case of bulk polymer materials, since they can be considered as isotropic half spaces. In the case of the grafted chains and the spin coated samples, substrate effects can come into play during the course of indentation. Although the used substrate materials have different Young's moduli (79 GPa for gold substrate and 130 GPa for the silicon wafer), they can be considered as equally stiff since AFM nanoindentation cannot distinguish between them according to Tsukruk.[48] In order to compare all the indentation data and to minimize, as far as possible, the effect of the stiff gold/silicon substrate (which will be discussed further in the following section), only the results of nanoindentation experiments with a low penetration depth (roughly 10 nm) were considered for modulus measurements.[49−51]

Figure 2 shows the average values obtained from 20 nanoindentations on each sample. An elastic modulus of ~3 GPa was calculated in most of the cases, i.e., for macroscopic DMTA tests,[46] for nanoindentation on bulk PMMA[46] and for the 150 nm thick spin-coated samples (this work). An even higher modulus was observed for the 70 nm thin spin-coated sample.

By applying the same procedure used for the bulk and spin-coated samples, an equivalent nanoindentation modulus can be calculated for both the PMMA brushes in order to quantify the differences in the elastic behavior (Figure 2).

Further experimental observations confirm the enhanced elastic behavior of grafted polymer, since the plastic behavior of the grafted brush sample was found to be significantly different. The unloading curves are not shown here because the combination of viscoelastic phenomena and the sharp indenter used for AFM nanoindentations, much sharper than the indenters used for depth sensing instruments, render the AFM unloading curves poorly understood.[52] As an alternative, we analyzed the images collected on the samples after the nanoindentation. In this case, plasticity during nanoindentation manifests itself obviously with the residual imprint left behind the indenter, but also with pile-up,[53] i.e., the bulging out of the surface due to plastic flow.

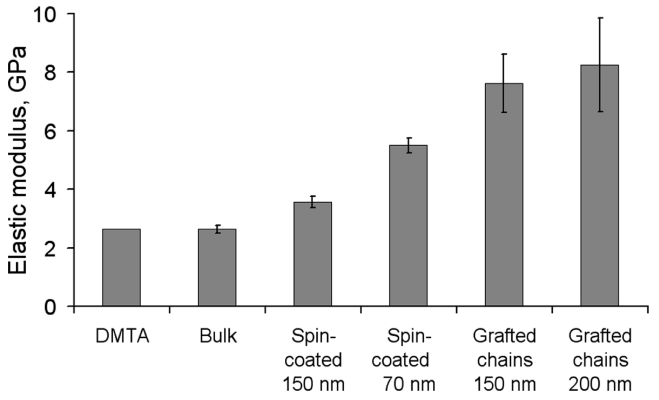

Figure 2. Comparison of the Young's moduli obtained on 5 different PMMA samples with both DMTA and AFM nanoindentations. The data for the bulk modulus determined by DMTA and by nanoindentation were taken from ref 46. Considerable stiffening was found for the thin spin-coated sample and even more dramatic increase for the grafted chains.

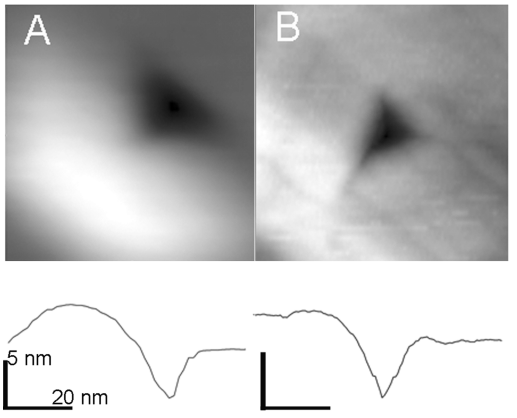

Figure 3. AFM images of the residual imprint left behind the indenter (120 nm × 120 nm), (A) for the spin-coated PMMA film (thickness 70 nm) after nanoindentations performed at 3.28 μN, and (B) the grafted PMMA brush sample after an indentation at 3.90 μN, respectively. The corresponding profiles along the direction of maximum residual depth and pile-up height are shown at the bottom.

Two representative images of the residual imprints, obtained by scanning with the same AFM tip that performed the nanoindentation, are shown in Figure 3, parts A and B, respectively, for the spin-coated and grafted brush sample. It is worth to stress that these imprints were obtained after nanoindentation that implied a penetration depth under full load in the order of 40 nm, therefore experimental conditions are completely different than the ones used for obtaining the values of Young's moduli of Figure 2. The pile-up is more pronounced on one side of the indent since the AFM tip is not symmetric, and higher stresses can be expected along the sharp edges. The respective profiles cut along the direction of maximum residual depth show that the same residual depth was obtained in this case, ~10 nm. However, this was obtained after applying a load of 3.28 μN in the case of the 70 nm thick spin-coated sample and by contrast, a higher load of 3.90 μN was required to achieve the same residual indentation depth for the brushes. In this latter case we observed an increase of 40% for the plastic load. Moreover, results not shown here indicate that a load as high as 6.0 μN is required to induce the same vertical pile-up for the grafted PMMA brushes. The increased load needed to induce the same residual depth suggests the enhanced recovery of grafted chains as compared to the entangled, spin-coated sample.

In general, a dramatic softening is observed for polymers after yield, due to the combined effect of strain and thermal softening. Arruda et al.[54] showed that the stress in stress−strain curves of

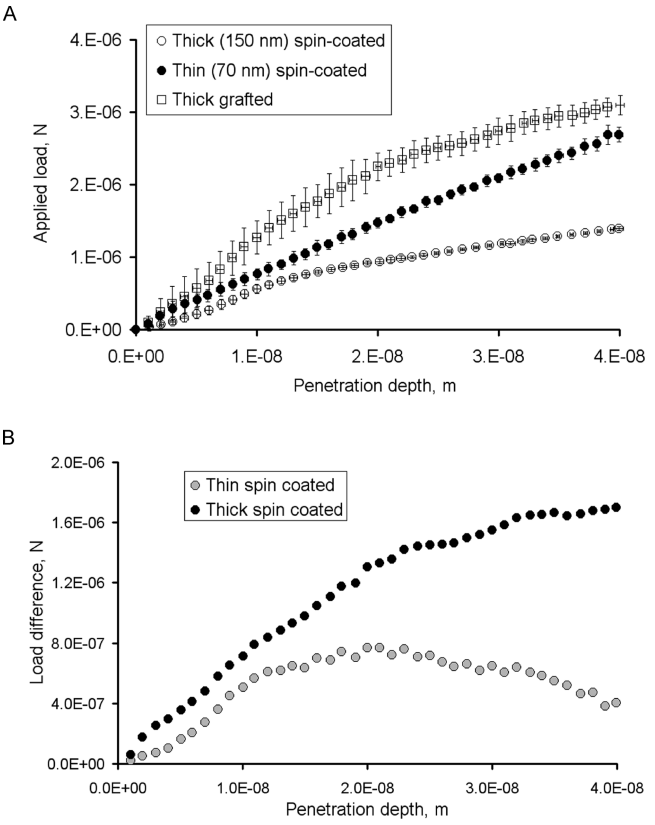

Figure 4. Averages of 20 force curves obtained from AFM nanoindentation measurements of the thin and thick spin-coated and the grafted PMMA samples (A). Compared to the spin-coated films, the raw data shows a stiffer behavior for the brush sample. Part B shows the contribution of entropy change to the stress field expressed as overall applied load, obtained as the difference between the loads of the grafted and respectively thin (gray series) or thick (black series) spin coated in part A.

PMMA in tension falls remarkably after yielding in the case of fast tests, from 140 MPa at yield to 90 MPa after it. Incidentally, the yield stress is highly enhanced as well,[54] and this finding explains the prevailing elastic constant and the high value for the elasticity parameter ξ discussed above.

Because of the anisotropically strengthened components, the grafted film is expected to require a higher load to result in the same deformation, when compared to the spin-coated one. Moreover, it is expected that the isotropic glassy polymer macromolecular structure, which forms a network by virtue of physically entangled molecular chains, evolves with the magnitude and state of strain during deformation as secondary valence interactions dissociate with plastic strains.[54]

On the other hand, for the PMMA brushes, the deformation of stretched chains is more difficult at relatively low penetration depth, while upon deformation a softer material is created as the composite of highly stretched and coiled chains.

In Figure 4A, three averaged nanoindentation curves are shown for the grafted brushes and the two spin coated samples. These curves were calculated from 20 individual force curves for each sample. Compared to the spin-coated PMMA films, the PMMA brushes were found to be stiffer. The difference in applied load needed to achieve a certain penetration depth is shown in Figure 4B.

3. Substrate Effect

As mentioned above, the method used to extract the modulus of the film from indentation data is based on a model valid for isotropic homogeneous solids. In the case of a coated substrate, a so-called "equivalent elastic modulus", E_{eq}, is obtained through

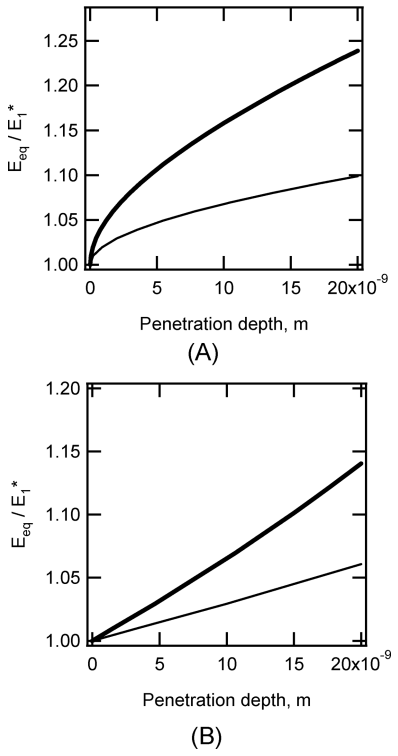

Figure 5. Calculated equivalent indentation modulus as a function of the penetration depth in the case of the elastic indentation of a frictionless coated substrate by (A) a sphere and (B) a cone. The equivalent modulus is normalized with respect to the modulus of the layer, E_1*. Bold line: 70 nm. Plain line: 150 nm. The ratio of the reduced modulus of the substrate to that of the layer, E_0*/E_1*, is set to 38 in the calculations. Penetration depths were calculated assuming a radius R = 10 nm for the sphere and a half included angle of 35 deg for the cone.

this method which is a combination of the respective moduli of the film, E_1, and of the substrate, E_0. As pointed out by Doerner and Nix,[55] the relative weight of the substrate and coating contributions to this equivalent modulus varies with penetration depth. In order to evaluate substrate effects on the measurement of the Young's modulus of spin-coated and grafted films, elastic contact mechanics calculations have been carried out along the lines of an exact semianalytical model developed for coated substrates by Perriot and Barthel.[31b] In this model, solutions are provided for the load and penetration of a frictionless coated contact indented by a cone or a sphere. Calculations were carried out using a ratio of the reduced modulus of the substrate to the reduced modulus of the film, E_0*/E_1*, equal to 38 (where E_i* = $E_i/(1-\nu_i^2)$ and ν_i are respectively the reduced modulus and the Poisson's ratio of the film (i = 1) or the substrate (i = 0). This ratio corresponds to indentation of a glassy polymer layer (E_1 = 3 GPa, ν_1 = 0.4) lying on a silicon substrate (E_0 = 130 GPa and ν_0 = 0. 2). For the low indentation depth (i.e., 10 nm) used for the determination of the modulus, the AFM tip can be assimilated to a sphere with a radius of curvature of roughly 10 nm. Figure 5a shows the changes in the normalized equivalent modulus, E_{eq}*/E_1*, as a function of the indentation depth for the two films thicknesses (70 and 150 nm) achieved with the spin coated samples. As expected, the equivalent modulus is higher for the 70 nm film than for the 150 nm film as substrate effects are more pronounced. However, it turns out that, in both cases, substrate effects induce a limited deviation of the calculated equivalent modulus from the Young's modulus of the layer. For a 10 nm indentation depth, the ratio E_{eq}*/E_1* is equal to only 1.16 for the thinnest (70 nm) film. In other words, substrate effects induce an error (16%) in the determination of the actual Young's modulus of the layer which

Table 1. Calculated Equivalent Reduced Modulus as a Function of Film Thickness in the Case of Cone and Sphere Indentation of a Coated Substrate[a]

film thickness (nm)	type	E_{eq}*/E_1*
70	cone	1.06
150	cone	1.03
70	sphere	1.16
150	sphere	1.07

[a] The equivalent modulus is calculated for a 10 nm indentation depth.

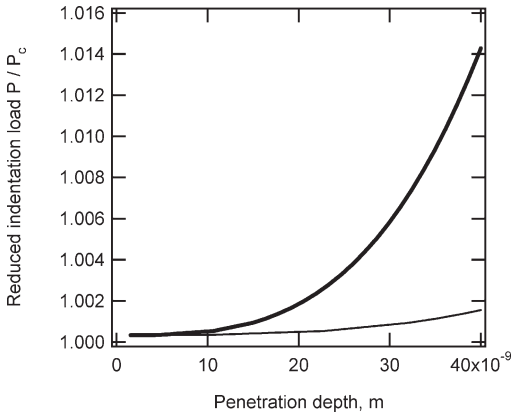

Figure 6. Calculated normalized indentation load, P/P_c, as a function of the indentation depth in the case of the elastic indentation of a coated substrate by a cone (E_0*/E_1* = 38, β = 35 deg). Bold line: 70 nm. Plain line: 150 nm.

is of the order of magnitude of experimental uncertainty (about 10−15% depending on the film specimen) and cannot justify the considerable differences of mechanical properties among the films with different morphologies observed in Figure 2. This conclusion is preserved if cone indentation is considered instead of sphere indentation (Figure 5b and Table 1). As a conclusion, it can be stated that substrate effects do not significantly affect the Young's modulus measured using Sneddon's model at the considered low penetration depth. Differences between the different spin-coated and grafted films can be therefore considered as representative of different mechanical response of these films.

Additional calculations were carried out at increased indentation depths using the cone geometry for indentation depths up to 40 nm, which correspond to the experimental data reported in Figure 4. In Figure 6, the normal load, P, normalized with respect to its value for a semi-infinite body, $P_c = \pi a^2/2E_1^* tan\beta$ (where β is the half included cone angle), is represented as a function of the penetration depth. It emerges that substrate effects induce only a minor deviation from the load, P_c, corresponding to semi-infinite substrate. Although these calculations correspond to an elastic contact situation, one does not expect substrate effects to be substantially enhanced when plastic deformation is involved. Differences in the experimental plastic indentation behaviors reported in Figure 3 can thus be considered as truly representative of the yield response of the polymer layers.

4. Discussion

Since the radius of gyration can be estimated to be in the range of 10−15 nm, it might be surprising that the two spin coated samples result in very different moduli. Tweedie et al.[51] showed that an increase in stiffness for nanoindentations at low contact depths was observed for glassy polymers, which was independent of processing, thermal history, macromolecular structural properties, and humidity. These authors argued that the increase in stiffness was related to a polymer surface stiffening mechanism, due to the creation of a mechanically unique interfacial region between the probe and the polymer surface. Confinement arising

from decreased film thickness can further boost this phenomenon, since the effect of the stiff interphase is larger for small film thickness. This effect was consistently absent for the 150 nm thick spin-coated films.

When comparing the 150 nm thick spin-coated films with the PMMA brush, a marked increase of Young's modulus of three times was observed, even though the films possess comparable thickness. The 70 nm thin spin-coated film also showed a significant decrease of roughly 30% in modulus compared to the PMMA brush sample (150 nm thick). Indeed, in this latter case, it can be intuitively understood that the deformation in the direction of the chain is more difficult when compared to lateral deformations. The 30% increase observed for the glassy brush sample at room temperature is consistent with the results reported on brush and spin-coated PMMA above the glass-to-rubber transition by Urayama et al.[23]

Thorough studies have been performed in order to explain the novel behavior and morphology of tethered polymer brushes.[56] In particular, it has been shown that macromolecules in polymer brushes exhibit deformed configurations, i.e., they are stretched, as a result of the balance between the energetic interactions and the reduction in configurational entropy.[57] Therefore, deforming stretched macromolecules in a polymer brush during nanoindentation leads to an increase of entropy. Drozdov elegantly showed that in the case of tethered chains "the conventional entropic elasticity theory may lead to conclusions that contradict our physical intuition".[58] The increase in entropy inferred from the data in Figure 4 is corroborated by data obtained by indenting along an oblique direction (12° with respect to the surface normal direction). We observed, as shown in the Supporting Information (Figure S-2), that the grafted polymer behaves softer than the spin-coated polymer. The grafting density of the polymers comprising the brush was not determined in this study since the planar substrates did not yield enough material for standard GPC analyses.

Unlike for rubbery polymer systems, for which entropy elasticity is important, PMMA is described here by concepts of energy elasticity. After Landau,[59] the change of internal energy per unit volume, $\mathcal{E}$, upon mechanical deformation can be written as the difference between the work done by external forces ($\sigma\, d\varepsilon$) and the heat per unit volume ($T\, \mathrm{d}S$):

$$d\mathcal{E}^{grafted} = T\, \mathrm{d}S^{grafted} + \sigma_{ij}^{grafted}\, \mathrm{d}\varepsilon_{ij}^{grafted} \quad (1)$$

$$\mathrm{d}\mathcal{E}^{spincoated} = \sigma_{ij}^{spincoated}\, \mathrm{d}\varepsilon_{ij}^{spincoated} \quad (2)$$

where T denotes temperature and S entropy and where σ_{ij} and ε_{ij} are the components for the stress and strain tensors, respectively. Detailed experiments on isotropic glassy PMMA below the glass-to-rubber transition showed that entropic contributions to elastic response are minor, for example in the case of hydrostatic compression.[60,61] Therefore, the entropic term for a reversible isothermal deformation of *isotropic* PMMA (compare eq 2). can be neglected. Moreover, for macroscopic tests, nearly adiabatic conditions were found when the overall deformation up to rupture took up to 10 s.[54] Fischer-Cripps showed that a negligible increase in temperature is experienced by the material during nanoindentation.[62,63]

By contrast, the polymer brushes studied here are certainly anisotropic. Since substrate effects and the oedometric nature[31] of the contact, i.e., the elastic response of the constrained material discussed in Figure 2, can be ruled out as origin for the observations, a reasonable assumption is that the different behavior among the two samples arises solely due to entropic effects. In principle, a change in Young's modulus, as shown in Figure 2, implies that the contribution of the term $\sigma d\varepsilon$ is different for the two samples. However, it can also be supposed that this change in modulus arises only because of entropic effects, therefore belonging to the term $T\, \mathrm{d}S$. This is equivalent to assuming that the stress experienced by the grafted brush sample during nanoindentation has a further entropic contribution with respect to the spin-coated sample. This contribution lowers the effective stress acting on the sample and therefore increases the apparent nanoindentation elastic modulus, when the sample is indented vertically:

$$\sigma_{ij}^{grafted} \approx \sigma_{ij}^{spincoated} - T\frac{\partial S}{\partial \varepsilon_{ij}^{grafted}} \quad (3)$$

The contributions of this "entropic" stress field expressed as overall applied load (obtained as the mere difference between the loads in Figure 4A) are reported in Figure 4B.

Unfortunately, there are no contact mechanics theories available that allow one to quantify the stress field tensor of an AFM nanoindentation with sufficiently good approximation to estimate $\partial S/\partial \varepsilon$. In order to describe the entropy change during nanoindentation, we only considered the vertical stress, where it is highest, i.e., inside the contact area at the apex of the tip ($\rho = 0$ in eq 4). These stresses indeed compress the chains vertically, not allowing them to bend and rather force them to assume a more coiled configuration, thus increasing the entropy.

After Sneddon,[47] we write the stress in the z direction in cylindrical coordinates for the case of nanoindentation with a paraboloid as follows:

$$\sigma_{zz}(\rho, 0) = -\frac{4\mu p}{\pi a^2(1-\nu^2)}\sqrt{a^2-\rho^2}, \quad \rho < a \quad (4)$$

Here a is the contact radius, p is the penetration depth, ν is the Poisson's ratio, and μ is the first Lamé coefficient, which contains the Young's modulus.

Sneddon also showed that the ratio of penetration depth and contact radius p/a in eq 4 is equal to the square root of the ratio of the penetration depth and tip radius. Following eqs 2−4 for $\rho = 0$, and assuming that the strain is proportional to the square root of the ratio of penetration depth and tip radius, while the spin-coated PMMA and the grafted one differ only in the values of Young's moduli, a qualitative change in conformational entropy per unit strain, $\partial S/\partial \varepsilon$, with increasing penetration depth was estimated.

Since only the stress at the apex of the tip, which is fairly high compared to the overall stress field, is taken into account, the values obtained are not absolute and were hence plotted in arbitrary units. By integrating $\partial S/\partial \varepsilon$, it is found that the increase in entropy is given by

$$\int_0^{\varepsilon\max} \frac{4p}{\pi a(1-\nu^2)T}\Delta\mu\, \mathrm{d}\varepsilon = \int_0^{p\max} \frac{4}{\pi(1-\nu^2)T}\sqrt{\frac{P}{R}}\Delta\mu\, \mathrm{d}\left(\sqrt{\frac{P}{R}}\right) \quad (5)$$

where R is the tip radius.

The overall entropy is found to increase with increasing penetration depth for the tethered chains (Figure 7A), both when comparing their stress field to the thick and to the thin spin coated films. These findings agree with calculations that show that the internal energy of the sample increases monotonically with strain as the isotropic material is transformed into oriented material during the deformation process.[64]

Figure 7B correctly shows that the entropy increase, because of tethered chains unstretching, causes the apparent load contribution to the force curve, to different extents whether the brush force curves are compared to the thin or to the thick sample.

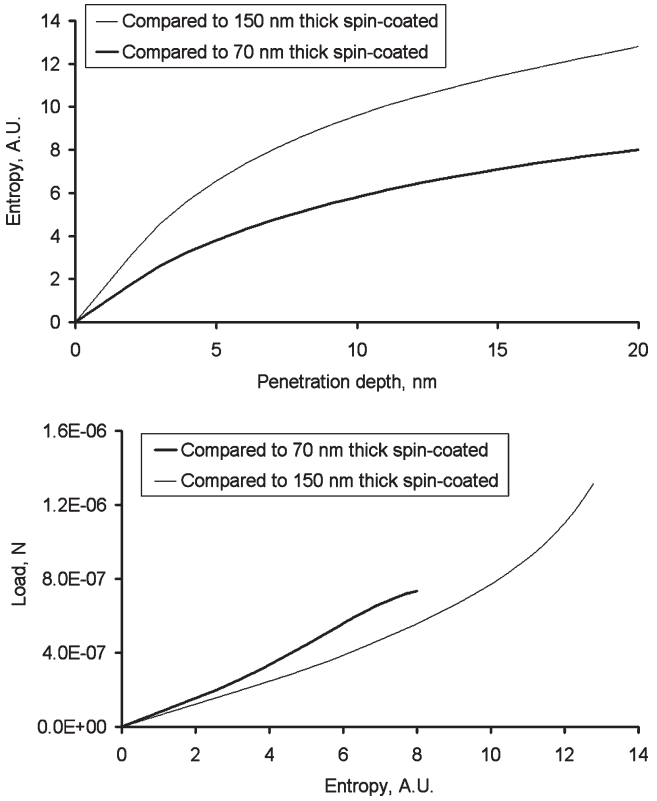

Figure 7. Entropic effects on nanoindentations of grafted chains. The overall entropy change was obtained after evaluating the stresses with Sneddon's model (details: see text).

5. Conclusions

In conclusion, grafted PMMA chains show enhanced elastic and plastic behavior, when compared to spin-coated samples. The reason can be found, according to the thermodynamics of deformation, in entropic effects that were shown to be responsible for an apparent stress contribution that lowers the stress experienced by the sample. Moreover, when the directionality is lost, e.g., by indenting along an oblique direction, the entropy-based stiffening effect disappears and the grafted polymer behaves softer. This finding is reasonable when considering that tethered chains represent a highly anisotropic system. The peculiar anisotropic deformation behavior unraveled in this current study for PMMA and the assignment of the entropic origin can very likely be generalized to account for the behavior of brushes of other amorphous polymers. Our results highlight the need of further studies of nanomechanical properties of polymeric brushes in view of applications where the deformation direction varies or is uncontrolled. Moreover, it is shown that changes of surface thermodynamic properties can be induced by deformation, which possesses very likely relevance for the unusual reactivity observed in micro- and nanoscale contacts[65,66] or for nanotribology of hydrated brushes,[67] among others.

6. Experimental Section

Spin-Coated PMMA Films. PMMA with a molar mass of 33 000 g mol^{-1} was used as received (Aldrich) and dissolved in toluene to yield solutions with concentrations of 20 and 45 mg/mL. The solutions were spin-coated at 3000 rpm on a precleaned silicon wafer using a home-built spin-coater. The films obtained were annealed for 1 h at 130 °C. The thicknesses of the films of 70 and 150 nm were estimated from AFM step height analyses of defined scratches in the films.

PMMA brushes. Methyl methacrylate (MMA, 99%), mercaptoundecanol (97%), pyridine (99%), bromoisobutyryl bromide (98%), copper(I) bromide (99.99%), and 2,2′-bipyridyl (99+%) were obtained from Aldrich. MMA was passed through an alumina column to remove the inhibitor; all other materials were used as received. ω-Mercaptoundecyl bromoisobutyrate was synthesized according to the literature.[68] Polymer brush growth was achieved by placing the substrates, modified by microcontact printing with the bromoisobutyrate-terminated initiator, in a Schlenk tube under an argon atmosphere and adding a degassed solution of MMA (10 g, 100 mmol), CuBr (143 mg, 1.0 mmol), and 2,2′-bipyridine (312 mg, 2.0 mmol), in the solvent mixture (deoxygenated Milli-Q water (2 mL) and MeOH (8 mL)) by cannulation. The polymerization was then allowed to proceed overnight at room temperature, after which removing the substrates from the reaction flask stopped the reaction. The substrates were extracted overnight with cold methanol in a Soxhlet apparatus with solvent cooling unit.

Atomic Force Microscopy. Nanoindentation was performed with a Nanoscope IIIA (Veeco, Santa Barbara, CA) under different applied loads and at tip indenting rate of 18 μm s^{-1}. Olympus OMCL-AC160TS cantilevers were used. A tip radius of 10 nm was estimated before nanoindentations by blind estimation[69] using an AFM height image $5 \times 5\ \mu m^2$ obtained on a standard calibrating sample (TGT01, NT-MDT, Moscow, Russia). The cantilever spring constant of 43 ± 1 N/m, was estimated from the resonance frequency. Moreover, standard tipless cantilevers (Applied Nanostructures, Santa Clara, CA) were used to cross-check this value. The cantilever deflection sensitivity, 51 ± 1 nm/V, was checked before and after the nanoindentation measurements on a stiff Si substrate, always giving consistent results.

Acknowledgment. D.T. acknowledges generous financial support of the Alexander von Humboldt Stiftung, Germany.

Supporting Information Available: Determination of brush thickness by AFM, AFM nanoindentation measurements for indentation in an oblique direction, values of normalized standard deviation vs number of indentations. This material is available free of charge via the Internet at http://pubs.acs.org.

References and Notes

(1) Barbey, R.; Lavanant, L.; Paripovic, D.; Schüwer, N.; Sugnaux, C.; Tugulu, S.; Klok, H.-A. *Chem. Rev.* **2009**, *109*, 5437.
(2) Bhattacharya, A.; Misra, B. N. *Prog. Polym. Sci.* **2004**, *29*, 767.
(3) Jain, P.; Baker, G. L.; Bruening, M. L. *Annu. Rev. Anal. Chem.* **2009**, *2*, 387.
(4) Ducker, R.; Garcia, A.; Zhang, J. M.; Chen, T.; Zauscher, S. *Soft Matter* **2008**, *4*, 1774.
(5) Edmondson, S.; Osborne, V. L.; Huck, W. T. S. *Chem. Soc. Rev.* **2004**, *33*, 14.
(6) Dutta, N.; Green, D. *Langmuir* **2008**, *24*, 5260.
(7) Xu, X.; Cao, D. J. *Chem. Phys.* **2009**, *130*, 164901.
(8) Zdyrko, B.; Klep, V.; Li, X.; Kang, Q.; Minko, S.; Wen, X.; Luzinov, I. *Mater. Sci. Eng., C* **2009**, *29*, 680.
(9) Vyas, M. K.; Nandan, B.; Schneider, K.; Stamm, M. *J. Colloid Interface Sci.* **2008**, *328*, 58.
(10) Zhao, B.; Brittain, W. J. *Prog. Polym. Sci.* **2000**, *25*, 677.
(11) Dimitrov, D. I.; Milchev, A.; Binder, K. *J. Chem. Phys.* **2007**, *127*, 084905.
(12) Huck, W. T. S. *Chem. Commun.* **2005**, 4143.
(13) Ohno, K.; Sakamoto, T.; Minagawa, T.; Okabe, Y. *Macromolecules* **2007**, *40*, 723.
(14) Keddie, J. L.; Jones, R. A. L.; Cory, R. A. *Europhys. Lett.* **1994**, *27*, 59.
(15) Alcoutlabi, M.; Mc Kenna, G. B. *J. Phys.: Condens. Matter* **2005**, *17*, 461.
(16) Schönherr, H.; Tocha, E.; Vancso, G. J. *Top. Curr. Chem.* **2008**, *285*, 103.
(17) Priestley, R. D.; Ellison, C. J.; Broadbelt, L. J.; Torkelson, J. M. *Science* **2005**, *309*, 456.
(18) Prucker, O.; Christian, S.; Bock, H.; Ruhe, J.; Frank, C. W.; Knoll, W. *Macromol. Chem. Phys.* **1998**, *199*, 1435.

(19) Watanabe, H.; Tirrel, M. *Macromolecules* **1993**, *26*, 6455. Taunton, H. J.; Toprakcioglu, C.; Fetters, L.; Klein, J. *Macromolecules* **1990**, *23*, 571.
(20) (a) O'Shea, S. J.; Welland, M. E.; Rayment, T. *Langmuir* **1993**, *9*, 1826. (b) Kelly, T. W.; Schorr, P. A.; Johnson, K. D.; Tirrel, M.; Frisbie, C. D. *Macromolecules* **1998**, *31*, 4297.
(21) Urayama, K.; Yamamoto, S.; Tsujii, Y.; Fukuda, T.; Neher, D. *Macromolecules* **2002**, *35*, 9459.
(22) Edwards, S. F.; Vilgis, T. A. *Polymer* **1986**, *27*, 483.
(23) Huang, H.; Young Chung, J.; Nolte, A. J.; Stafford, C. M. *Chem. Mater.* **2007**, *19*, 6555.
(24) Butt, H.-J.; Cappella, B.; Kappl, M. *Surf. Sci. Rep.* **2005**, *59*, 1.
(25) (a) Kim, M. S.; Pratt, J. R. *Measurement* **2010**, *43*, 169. (b) Kranenburg, J. M.; Tweedie, C. A.; van Vliet, K. J. *Adv. Mater.* **2009**, *21*, 3551.
(26) (a) Passeri, D.; Bettucci, A.; Biagioni, A.; Rossi, M.; Alippi, A.; Tamburri, E.; Lucci, M.; Davoli, I.; Berezina, S. *Ultramicroscopy* **2009**, *109*, 1417. (b) Cheng, Y. T.; Yang, F. Q. *J. Mater. Res.* **2009**, *24*, 3013. (c) Moeller, G. *J. Polym. Sci., B: Polym. Phys.* **2009**, *47*, 1573. (d) Gray, A.; Orecchia, D.; Beake, B. D. *J. Nanosci. Nanotechnol.* **2009**, *9*, 4514. (e) Keerthika, B.; Cao, Y. P.; Raabe, D. *CMC-Comput. Mater. Continua* **2009**, *10*, 243. (f) Bouaita, N.; Bull, S. J.; Palacio, J. F. *Polym. Eng. Sci.* **2006**, *46*, 1160. (g) Tranchida, D.; Kiflie, Z.; Piccarolo, S.; Acierno, S. *Meas. Sci. Technol.* **2009**, *20*, 095702.
(27) (a) Beayaoui, M.; Mazeran, P. E.; Arvieu, M. F. *Int. J. Mater. Res.* **2009**, *100*, 943. (b) Poon, B.; Rittel, D.; Ravichandran, G. *Int. J. Sol. Struct.* **2008**, *45*, 6399. (c) Poon, B.; Rittel, D.; Ravichandran, G. *Int. J. Sol. Struct.* **2008**, *45*, 6018. (d) Tranchida, D.; Piccarolo, S. *Polymer* **2005**, *46*, 4032. (e) Chizhik, S. A.; Huang, Z.; Gorbunov, V. V.; Myshkin, N. K.; Tsukruk, V. V. *Langmuir* **1998**, *14*, 2606.
(28) (a) Adhikari, R.; Michler, G. H. *Polym. Rev.* **2009**, *49*, 141. (b) Kranenburg, J. M.; Thijs, H. M. L.; Tweedie, C. A. *J. Mater. Chem.* **2009**, *19*, 222. (c) Bedoui, F.; Sansoz, F.; Murthy, N. S. *Acta Mater.* **2008**, *56*, 2296. (d) Jee, A. Y.; Kwon, H.; Lee, M. *J. Chem. Phys.* **2009**, *131*, 171104. (e) Tranchida, D.; Kiflie, Z.; Piccarolo, S. *Macromol. Rapid Commun.* **2006**, *27*, 1584.
(29) Lemieux, M.; Minko, S.; Usov, D.; Stamm, M.; Tsukruk, V. V. *Langmuir* **2003**, *19*, 6126.
(30) Zhao, J.; Chen, M.; An, Y.; Liu, J.; Yan, F. *Appl. Surf. Sci.* **2008**, *255*, 2295.
(31) (a) Gacoin, E.; Fretigny, C.; Chateauminois, A.; Perriot, A.; Barthel, E. *Trib. Lett.* **2006**, *21*, 245–252. (b) Perriot, A.; Barthel, E. *J. Mater. Res* **2004**, *19*, 600.
(32) Fretigny, C.; Chateauminois, A. *J. Phys. D* **2007**, *40*, 5418.
(33) Chen, S.; Liu, L.; Wang, T. *Acta Mater.* **2004**, *52*, 1089.
(34) Clifford, C. A.; Seah, M. P. *Nanotechnology* **2009**, *20*, 145708.
(35) Chen, J.; Bull, S. J. *Vacuum* **2009**, *83*, 911.
(36) Liao, Y.; Zhou, Y.; Huang, Y.; Jiang, L. *Mech. Mater.* **2009**, *41*, 308.
(37) Pelegri, A. A.; Huang, X. *Comput. Sci. Technol.* **2008**, *68*, 147.
(38) Zhao, M.; Chen, X.; Xiang, Y.; Vlassak, J.; Lee, D.; Ogasawara, N.; Chiba, N.; Gan, Y. X. *Acta Mater.* **2007**, *55*, 6260.
(39) Clifford, C. A.; Seah, M. P. *Nanotechnology* **2006**, *17*, 5283.
(40) Geng, K.; Yang, F.; Druffel, T.; Grulke, E. A. *Polymer* **2005**, *46*, 11768.
(41) Kopycinska-Müller, M.; Geiss, R. H.; Müller, J.; Hurley, D. C. *Nanotechnology* **2005**, *16*, 703.
(42) Zhao, M.; Xiang, Y.; Xu, J.; Ogasawara, N.; Chiba, N.; Chen, X. *Thin Solid Films* **2008**, *516*, 7571.
(43) Cappella, B.; Silbernagl, D. *Thin Solid Films* **2008**, *516*, 1952.
(44) Chen, S.; Liu, L.; Wang, T. *Surf. Coat. Technol.* **2005**, *191*, 25.
(45) Wang, M.; Liechti, K. M.; White, J. M.; Winter, R. M. *J. Mech. Phys. Sol.* **2004**, *52*, 2329.
(46) Tranchida, D.; Piccarolo, S.; Soliman, M. *Macromolecules* **2006**, *39*, 4547.
(47) Sneddon, I. N. *Int. J. Eng. Sci.* **1965**, *3*, 47.
(48) Tsukruk, V. V.; Gorbunov, V. V.; Huang, Z.; Chizhik, S. A. *Polym. Int.* **2000**, *49*, 441.
(49) Johnson, K. L. *Contact Mechanics*; Cambridge University Press: Cambridge, 2003.
(50) Silbernagl, D.; Sturm, H.; Cappella, B. *Langmuir* **2009**, *25*, 5091.
(51) Tweedie, C. A.; Constantinides, G.; Lehman, K. E.; Brill, D. J.; Blackman, G. S.; Van Vliet, K.J . *Adv. Mater.* **2007**, *19*, 2540.
(52) Tranchida, D.; Piccarolo, S. *Macrom. Rapid Commun.* **2005**, *26*, 1800.
(53) Tranchida, D.; Piccarolo, S.; Loos, J.; Alexeev, A. *Macromolecules* **2007**, *40*, 1259.
(54) Arruda, E. M.; Boyce, M. C.; Jayachandran, R. *Mech. Mater.* **1995**, *19*, 193.
(55) Doerner, M. F.; Nix, W. D. *J. Mater. Res.* **1986**, *1*, 601.
(56) (a) Milner, S. T.; Whitten, T. A.; Cates, M. E. *Macromolecules* **1989**, *22*, 1951. (b) Alexander, S. J. *J. Phys.* (*Paris*) **1977**, *38*, 977.
(57) Flory, P. J. *Principles of Polymer Chemistry*; Cornell University Press: Ithaca, NY, 1981.
(58) Drozdov, A. D. *Int. J. Eng. Sci.* **2005**, *43*, 1121.
(59) Landau, L. D., Lifshitz, E. M. *Theory of Elasticity*; Pergamon Press: New York, 1986.
(60) Theodorou, D. N.; Suter, U. W. *Macromolecules* **1986**, *19*, 139.
(61) Koppelmann, J.; Leder, H.; Royer, F. *Colloid Polym. Sci.* **1979**, *257*, 673.
(62) Fischer-Cripps, A. C. *J. Mater. Sci.* **2004**, *39*, 5849.
(63) Fischer-Cripps, A. C. *Nanoindentation*: Springer: Berlin, 2002.
(64) Oleinik, E. T. F.; Rudnev, S. N.; Salamatina, O. B.; Kotelyanskii, M. I. *Polym. Sci. Ser. A* **2008**, *50*, 494.
(65) Sullivan, T. P.; van Poll, M. L.; Dankers, P. Y. W.; Huck, W. T. S. *Angew. Chem., Int. Ed.* **2004**, *43*, 4190.
(66) Feng, C. L.; Embrechts, A.; Bredebusch, I.; Schnekenburger, J.; Domschke, W.; Vancso, G. J.; Schönherr, H. *Adv. Mater.* **2007**, *19*, 286.
(67) Drobek, T.; Spencer, N. D. *Langmuir* **2008**, *24*, 1484.
(68) Jones, D. M.; Brown, A. A.; Huck, W. T. S. *Langmuir* **2002**, *18*, 1265.
(69) Tranchida, D.; Piccarolo, S.; Deblieck, R. A. C. *Meas. Sci. Technol.* **2006**, *17*, 2630.